analytical chemistry

pubs.acs.org/ac Article

Tunable Dual-Effector Allostery System for Nucleic Acid Analysis with Enhanced Sensitivity and an Extended Dynamic Range

Liangliang Liu,‖ Mengmeng Yuan,‖ Yuxia Jin, Guobao Zhou,* Tuqiang Li, Lei Li,* Huaping Peng,* and Wei Chen

Cite This: *Anal. Chem.* 2021, 93, 8170−8177 Read Online

ACCESS | Metrics & More | Article Recommendations | Supporting Information

ABSTRACT: In the last few years, studies have demonstrated the existence of dual-effector allosteric cooperativity in nature and the mechanism underlying enhanced activation/inhibition performance. In this work, we design an artificial dual-effector allostery system for the construction of a dynamic biosensor that can achieve nucleic acid detection with superior sensitivity and across an extraordinary broad detection range. Our dual-effector allostery-regulated biosensor is based on the multibranched hybridization chain reaction (mHCR) involving three hairpins (H1, H2, and H3). In the presence of the target nucleic acid, the mHCR is initiated via cascading strand displacement events. The products of mHCR are then captured on the electrode surface based on the mechanism of the multivalent proximity ligation assay (mPLA) and the multivalent binding assay (mBA). The subsequent conjugation of streptavidin-modified horseradish peroxidase (SA-HRP) can lead to an increase in the electrochemical signal. Importantly, two distinct allosteric activation sites and two distinct allosteric inhibition sites in H1 are designed to fine-tune the nucleic acid detection sensitivity and the dynamic range. Using this new dual-effector allostery tool, we report the detection of nucleic acid at a dynamic range spanning 10−10^{12} aM, 11 orders of magnitude showing the broadest dynamic range reported to date with an allosteric regulation biosensor construct.

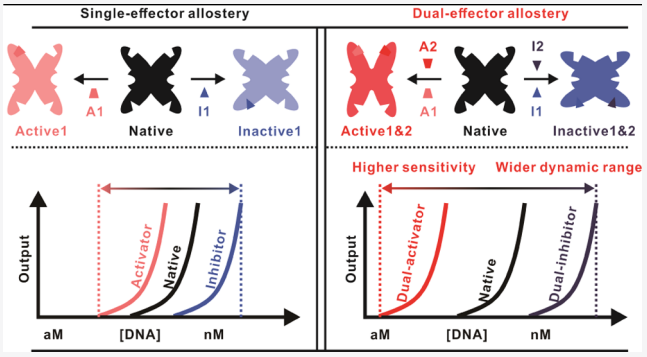

Biomarkers in clinical samples are probably present in trace abundance and their wide dynamic range are two of the main difficulties in the development of analytical platforms for sensitive, accurate, and reliable target analyte detection in liquid biopsy.[1,2] Biomarkers (e.g., proteins, cells, DNAs, RNAs, exosomes, and metabolites) show varying concentrations in different disease stages, initiation, and progression.[3−7] For instance, the dynamic range of proteins within the plasma is reported to surpass 10 orders of magnitude in many pathological and physiological processes.[8] Mitchell and co-workers reported that the sera levels of microRNA can distinguish cancer patients from healthy controls and the copy of miR-141 exhibits up to 4 orders of magnitude (10−100 000 copies) per microliter serum.[9] Besides, Wan and co-workers improved the detection of early stages of cancer by tracking hundreds of circulating tumor DNA mutations, which span a 10^6-fold range.[10]

However, most developed biosensors have a confined dynamic range. For example, synthetic biosensors based on antibody−probe affinity analysis are responsible for the detection of the biomarker in the range of concentrations around its equilibrium constant (K_d) value, such that their detection ranges are typically on 2 orders of magnitude (81-fold), and it is extraordinarily difficult to edit its dynamic range.[11] The fundamental restriction makes it difficult to deal with wide variations in biomarker concentration. Many researchers have designed strategies to shift the dynamic range of biosensors by precisely controlling probe affinity[12−20] (K_d value) or the programmable tuning signal output.[21−26] For example, by applying allosteric regulation- or mutation-based tools to modulate the affinity of target-binding probes, such as protein,[19,27] DNA hairpin,[14,15,28] aptamer,[12,13,16,29] DNAzyme,[17,18,30,31] and many other DNA nanostructures,[32−34] Hellinga, Ricci, and others have proposed a series of biosensors that can tune the detection range over 5 orders of magnitude. Moreover, Jang and co-workers achieved a dynamic biosensor through facile control of only the signaling probe concentration.[26] Nevertheless, there remains an urgent need for new strategies for the development of biosensors with ultrabroad detection ranges due to the wide dynamic ranges of many clinically relevant biomarkers, which can vary over more than 6 orders of magnitude.

Received: January 6, 2021
Accepted: May 5, 2021
Published: June 6, 2021

https://doi.org/10.1021/acs.analchem.1c00055
Anal. Chem. 2021, 93, 8170−8177

Dual allosteric regulation possessing enhanced activation/inhibition performance is a newly founded mechanism of allostery in recent years.[35−37] Brown and Thorpe demonstrated that hepatitis C virus polymerase exhibits increased therapeutics (improved inhibition performance) with two non-nucleoside inhibitors bound distal to the enzyme active site.[35] Ballicora and co-workers also founded that the dual-activator mechanism enhances the evolvability of ADP-glucose pyrophosphorylase (improved activation performance).[36] Here, we proposed a novel biosensor design based on the dual-effector allostery mechanism that target-binding probe H1 couples together two distinct allosteric activation sites and two distinct allosteric inhibition sites. When compared with the single-effector allostery system, the dual-effector allostery system enables nucleic acid detection with enhanced sensitivity and an extended dynamic range (Scheme 1). Using this new modulating approach, we prove that our biosensor can successfully analyze nucleic acid concentrations ranging from 10 aM to 1 μM, a dynamic range spanning more than 11 orders of magnitude representing the broadest target detection range reported to date for an allosteric regulation biosensor construct. Moreover, we combined the dual-activator positive regulation and the multivalent capture strategy (the combination of multivalent proximity ligation assay (mPLA) and multivalent binding assay (mBA)) to improve the capability of signal amplification and the efficiency of signaling product capture on the electrode surface, leading to a significant increase in nucleic acid detection sensitivity.

Scheme 1. Schematic Illustrations of Single-Effector Allostery and Dual-Effector Allostery Mechanisms[a]

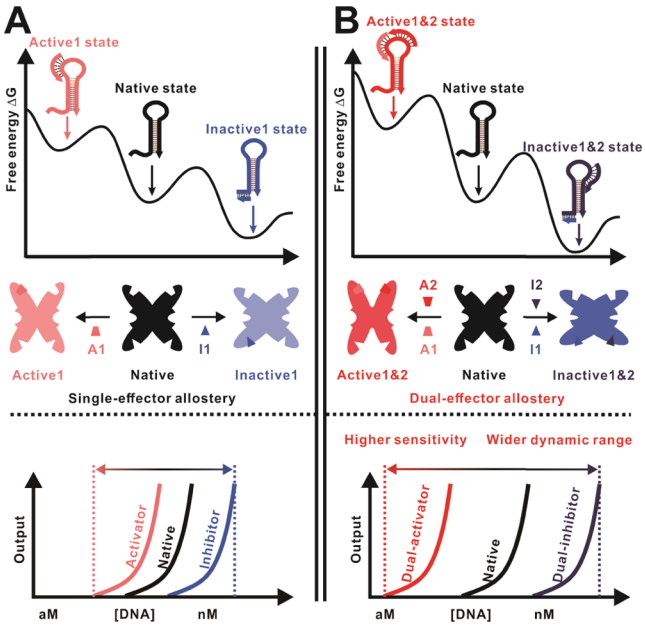

[a](A) H1 has an allosteric activation site in the loop and an allosteric inhibition site in the toehold. The binding of the activator improves the mechanical tension of H1 and induces an increase of free energy at the stem site. While the binding of the inhibitor to the toehold in H1 stabilizes the inactive state of H1 and decreases the free energy of H1. (B) H1 couples together two distinct allosteric activation sites in the loop and two distinct allosteric inhibition sites in the toehold and the loop. Similarly, the binding of activators improves the mechanical tension of H1 and induces an increase of free energy of H1. The binding of the inhibitors to the toehold and loop in H1 stabilizes the inactive state of H1 and reduces the free energy of H1. When compared with the single-effector allostery system, the dual-effector allostery system shows enhanced activation/inhibition performance.

EXPERIMENTAL SECTION

Materials and Reagents. DNA oligonucleotides used in this experiment (listed in Table S1) were synthesized, modified, and purified by Sangon Biotechnology Inc. GelRed, agarose, bovine serum albumin (BSA), casein, and reagents used to prepare different kinds of buffers were also purchased from Sangon. Tris(2-carboxyethyl) phosphine hydrochloride (TCEP) and 3,3′,5,5′-tetramethylbenzidine (TMB, slow kinetic form) were purchased from Sigma-Aldrich. Streptavidin−horseradish peroxidase (HRP) was obtained from Abcam. TM buffer (20 mM Tris, 50 mM $MgCl_2$, pH 8.0) was used to synthesize the tetrahedron DNA nanostructure. Phosphate-buffered saline (0.1 M) (PBS) (10 PB, 137 mM NaCl, 2.5 mM KCl, 0.05% Tween 20, pH 7.4) was used to rinse the electrode. SPSC buffer (1×) (50 mM PB, 1 M NaCl, pH 7.5) was used in the hybridization chain reaction. TBE buffer (1×) (40 mM of tris-acetate, 25 mM boric acid, and 1 mM ethylenediaminetetraacetic acid (EDTA)) was used in agarose gel electrophoresis (AGE) analysis. Stocking buffer (10 mM phosphate sodium buffer solution at pH 7.4, 0.1 M NaCl, 1% casein, 1% BSA) was used to dilute streptavidin−HRP.

Agarose Gel Electrophoresis Analysis. The DNA samples were mixed with appropriate loading buffer and were analyzed by the freshly prepared 2% agarose gel electrophoresis (AGE). The 2% agarose gels contained 0.01 μL of the GelRed of the gel volume and were prepared with 1× TBE buffer and were run at 150 V for 40 min and visualized under UV light (Gel Doc XR+, Bio-Rad).

Fluorescence Analysis. H1 (H1(fl)-inactive, H1(fl)-native, and H1(fl)-active) (1 μM) and H2 (1 μM) were heated separately at 95 °C for 5 min, allowed to cool at 4 °C within 60 s using an ABI Veriti96 thermal cycler, and then mixed with 0 or 5 nM target in 100 μL of 1× SPSC buffer for the final concentration 50 nM. The DNA hybridization chain reaction was carried out in 600 μL tubes for fluorescence spectra measurements. Time-dependent fluorescence monitoring was performed with a time interval of 1 s in a quartz cuvette on an F7000 spectrofluorometer (the excitation wavelength is 492 nm and the emission wavelength is 516 nm).

Electrocatalytic Analysis. H1 (H1(bio)-inactive, H1-(bio)-native, and H1(bio)-active) (5 μM) and (5 μM) H2 and H3 were heated separately at 95 °C for 5 min, allowed to cool at 4 °C within 60 s, and then mixed with different concentrations of the target (10 aM to 1 μM) in 100 μL of 1× SPSC buffer for the final concentration 100 nM. The hybridization chain reaction was carried out at room temperature. Gold electrodes were incubated with 3 μL of framework nucleic acids (FNAs) overnight at room temperature. The resulting electrodes were rinsed with PBS and then incubated with the above hybridization chain reaction solutions. SA-HRP (1 $\mu g \cdot mL^{-1}$) was finally added to bind with biotin on H1. The electrochemical measurement was tested in a slow kinetic TMB substrate at room temperature.

RESULTS AND DISCUSSION

Single-Effector and Dual-Effector Allostery System Mechanisms. We designed DNA hairpin (H1) variants with a diverse range of activated or inhibited affinities to the same

https://doi.org/10.1021/acs.analchem.1c00055
Anal. Chem. 2021, 93, 8170−8177

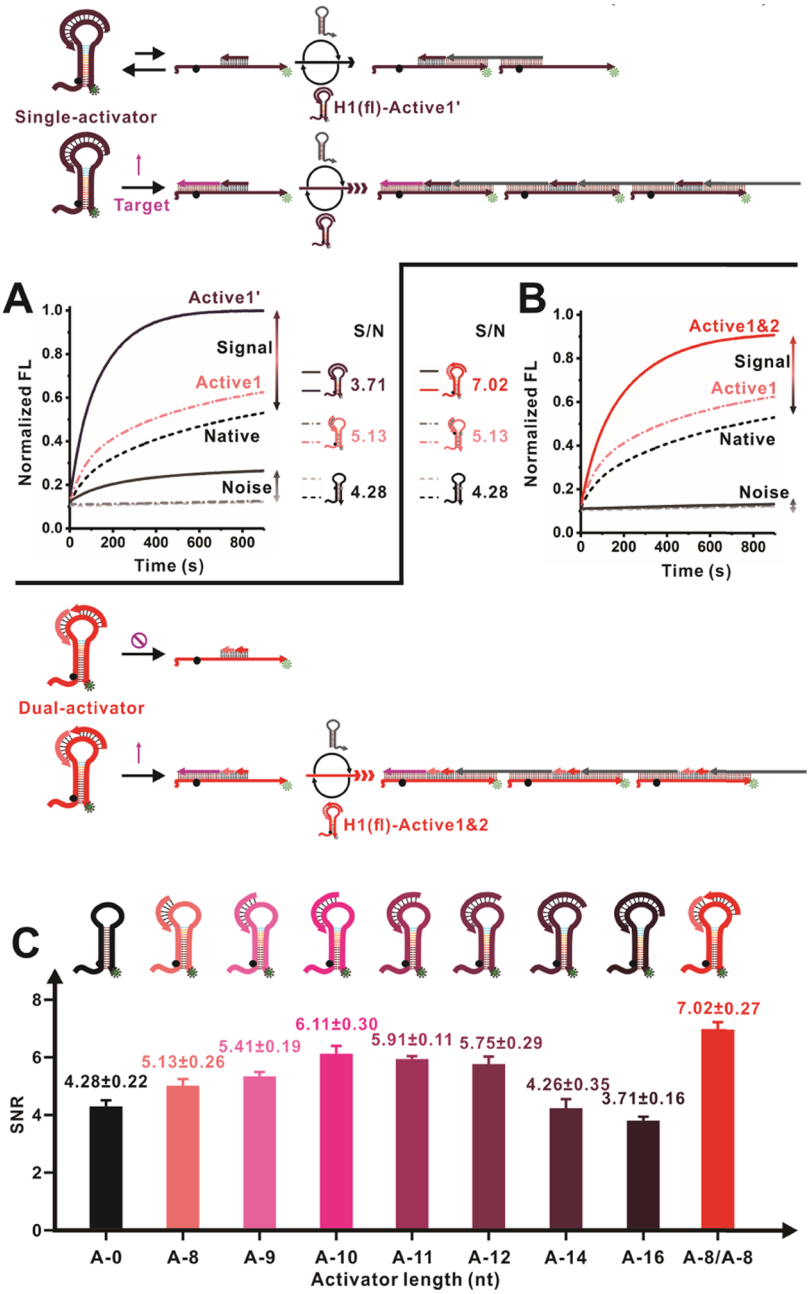

Figure 1. Kinetics of the hybridization chain reaction is accelerated by adding a single activator (A) or a dual activator (B). Target nucleic acids (0 and 5 nM) were introduced into the system at $t \approx 0$. The fluorescence intensity of each sample was monitored within 30 s of mixing by pipetting. Here, [H1(fl)] = [H2] = 50 nM. [Activator] = 1 μM. The noise trace and signal trace show the hybridization chain reaction induced with 0 and 5 nM targets, respectively. (C) Signal-to-noise ratio varies in the presence of different lengths of the single activator and the dual activator. The dual-activator allosteric system obtained an enhanced SNR when compared with the single-activator allosteric system.

target nucleic acid using single-effector allostery and dual-effector allostery. The activator, a short 8 nt to 16 nt single-stranded oligonucleotide that binds to the domain in the loop of H1, improves the mechanical tension and causes an increase of affinity at the stem site. The binding of the activator destabilizes H1, promoting the activity of the hybridization chain reaction (HCR). In contrast, the binding of the inhibitor (a short 8 nt single-stranded oligonucleotide) to the toehold in H1 stabilizes the inactive state of H1 and hinders the target nucleic acid displacement reaction, consequently decreasing the activities of HCR (Scheme 1A). Of note, there is a significant discrimination between activator cooperativity and inhibitor cooperativity. Inhibitor cooperativity can stabilize the inactive state, arbitrarily decreasing the background signal. On the contrary, activator cooperativity destabilizes the hairpin structure, increasing the background signal. Therefore, the activator cooperativity cannot be carried out ad infinitum, as the exceeded background signal finally reduces the performance of the dynamic biosensor. To further improve the performance of the dynamic biosensor using allosteric regulation, we introduce the dual-effector allosteric regulation instead of single-effector allosteric regulation in the construction of nucleic acid analyzing biosensors. There are two distinct allosteric activation sites and two distinct allosteric inhibition sites in H1. The binding of activator2 presents the same cooperative mechanism as activator1. The binding of

https://doi.org/10.1021/acs.analchem.1c00055
Anal. Chem. 2021, 93, 8170−8177

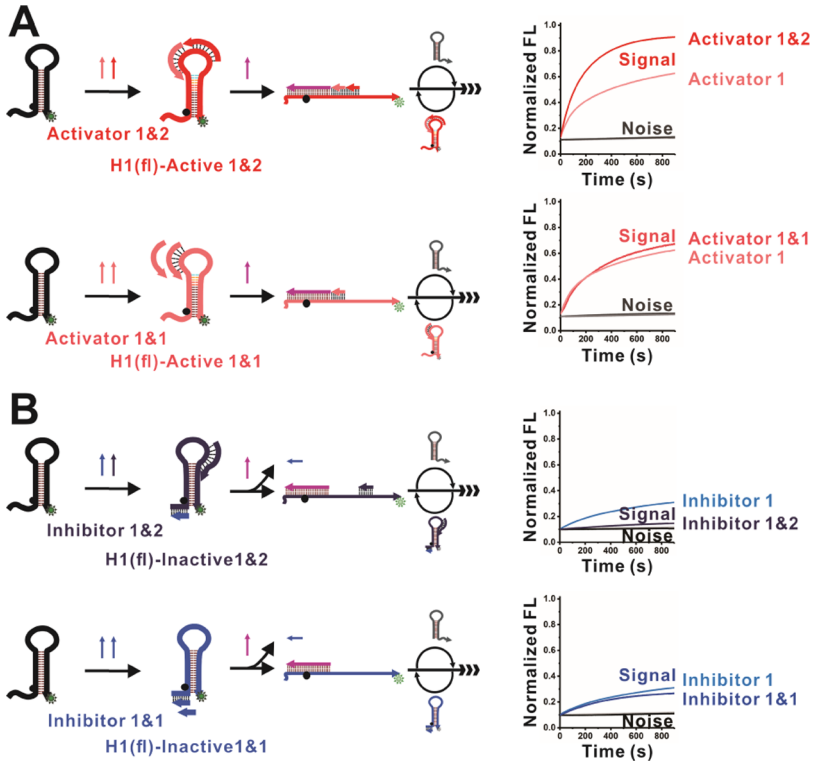

Figure 2. (A) Kinetics of the hybridization chain reaction is accelerated by adding 1 μM activator1 and 1 μM activator2 (top) or 2 μM activator1 (bottom). (B) Kinetics of the hybridization chain reaction is weakened by adding 1 μM inhibitor1 and 1 μM inhibitor2 (top) or 2 μM inhibitor1 (bottom). Here, [H1(fl)] = [H2] = 50 nM. The noise trace and the signal trace show the hybridization chain reaction induced with 0 and 5 nM targets, respectively.

inhibitor2 hinders the hybridization between opened H1 and H2. Overall, the binding of two activators and two inhibitors exhibits enhanced activation/inhibition performance and enables nucleic acid detection with enhanced sensitivity and an extended dynamic range (Scheme 1B).

Fluorescence Analysis Demonstration. To demonstrate the advanced performance of the dual-effector allostery system, we have conjugated H1 with a fluorophore/quencher pair such that, in the presence of target nucleic acid, FAM and dabcyl are separated upon a conformational change, resulting in the enhancement of the fluorescence intensity (Figure S1). As shown in Figure 1A,B, the dual-effector allosterically activated H1 obtained an improved signal-to-noise ratio (SNR) as expected. The binding of the 16 nt activator induced a significant increase in noise (0 nM target) fluorescence. When the 16 nt activator was cut into two 8 nt activators (activator1 and activator2), although both the noise fluorescence intensity and signal (5 nM target) fluorescence intensity decreased and the signal-to-noise ratio increased. In the single-effector allostery system, the kinetic rate of noise fluorescence intensity and signal fluorescence intensity both increased with the increase of the activator length (Figure 1C). We obtained the optimal signal-to-noise ratio using a 10 nt activator. Two 8 nt activators bound to H1 presented even better SNR, demonstrating the outstanding performance of dual-effector allostery in the dynamic biosensor construction.

The SNR at the same 5 nM target was increased by gradually increasing the activator concentration. We found that either the activator or the inhibitor exhibited saturated cooperativity at a concentration of 1 μM (Figures 2A,B (bottom) and S2). Moreover, we monitored the real-time fluorescence intensity of the hybridization chain reaction regulated by 1 μM activator1 and activator2 and 1 μM inhibitor1 and inhibitor2 (Figures 2A,B (top) and S3). We observed a higher rate constant for the dual-activator-cooperated HCR and a lower rate constant for the dual-inhibitor-cooperated HCR than that of the single-effector allostery-regulated HCR. These results further validated the superior performance of the dual-effector allostery system.

Electrocatalytic Analysis Procedures. Having demonstrated the advanced properties of the dual-effector allostery system, we then tried to analyze nucleic acids through an electrocatalytic assay, which is much more sensitive than the fluorescent method. Scheme 2 illustrates the nucleic acid detection processes via electrochemical measurement. H1, H2, and H3 are kept stable in hairpin structures until a specific target nucleic acid binding with H1 displaces the H1 stem and initiates the multibranched hybridization chain reaction. The conformational change of H2 transforms its inactive looped strand to an active linear strand. H2 can further hybridize with H3 through toehold displacement to obtain multibranched HCR products. Multibranched HCR products are captured by the probes on the vertex of framework nucleic acids (FNAs, Figure S4 proved the successful self-assembly of FNAs). Multiple streptavidin-modified horseradish peroxidases (SA-HRPs) were then conjugated to the biotins on multibranched HCR products, which generate remarkable electrocatalytic i−t current.

The high capture efficiency of mHCR products can further promote the sensitive detection of nucleic acid at ultralow concentrations. Except for the introduction of H3, 18 nucleotides were prolonged in H2 (10 nucleotides were used as a spacer) for generating multibranched HCR products. In the absence of the target, the H2 hairpin could not hybridize

https://doi.org/10.1021/acs.analchem.1c00055
Anal. Chem. 2021, 93, 8170−8177

Scheme 2. Schematic Illustrations of Nucleic Acid Detection through Electrochemical Measurement

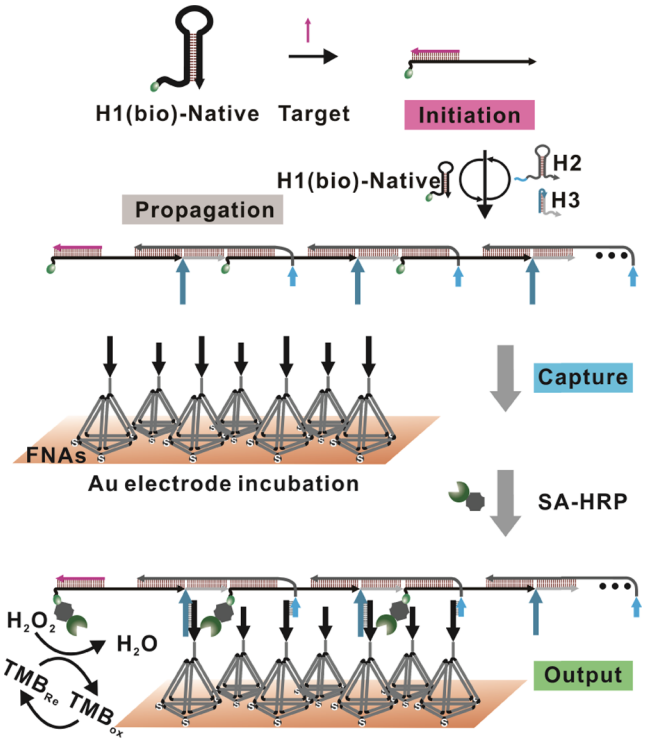

with the FNA probe. The FNA probe could get close to the HCR products with multibranched H2 proximity and dramatically increase their local effective concentrations, thereby improving the efficiency of the hybridization between multibranched H2 and FNAs.[38] We termed the hybridization between multibranched H2 and FNAs as multivalent proximity ligation assay (Figure 3A). The H3 hairpin also could not hybridize with the FNA probe in the absence of the target. As the HCR products with multibranched H3 could directly hybrid with the FNA probe, we termed it as multivalent binding assay (Figure 3B). We combined mPLA and mBA to enhance the capture efficiency of HCR products and obtained an optimal sensing performance when the ratio of H2 and H3 was 1:2 (Figure 3C).

AGE Analysis Demonstration. The multibranched HCR with or without H3 could be regulated by single-effector allostery and dual-effector allostery. Agarose gel electrophoresis (AGE) analysis shows that the average lengths or yield of the resulting multibranched HCR products are negatively or positively regulated by allosteric cooperativity. Also, the products of multibranched HCR regulated by dual the inhibitor and the dual activator are less and more than that regulated by the single inhibitor and the single activator, respectively, indicating the higher capability of dual-effector allostery cooperativity (Figures 4, S5, and S6). Besides, AGE analysis showed that the activity of multibranched HCR was gradually enhanced with the increase in the dual-activator concentration (Figure S7).

Dynamic Electrochemical Sensing Performance. We chose a 400 nM single activator and a 200 nM dual activator as optimal electrochemical sensing parameters because they showed the best SNR values (Figure S8). Then, we experimentally validated our capability to fine-tune the dynamic range of the electrochemical sensor using single-effector allostery, obtaining four different calibration curves for

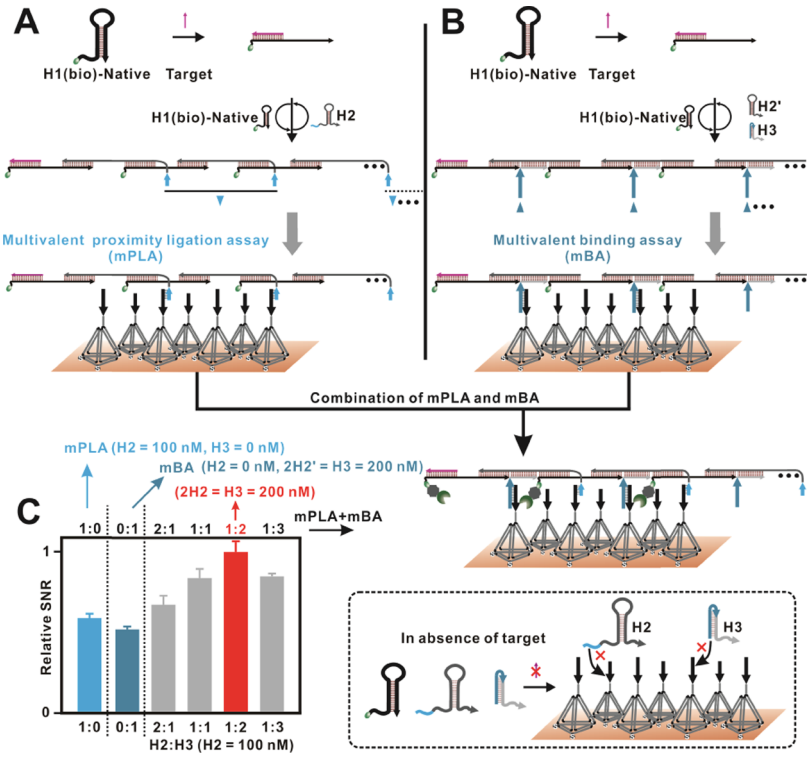

Figure 3. (A) mHCR products captured on the electrode surface through multivalent proximity ligation assay. (B) mHCR products captured on the electrode surface through multivalent binding assay. (C) mHCR products captured on the electrode surface through multivalent proximity ligation assay and multivalent binding assay.

https://doi.org/10.1021/acs.analchem.1c00055
Anal. Chem. 2021, 93, 8170−8177

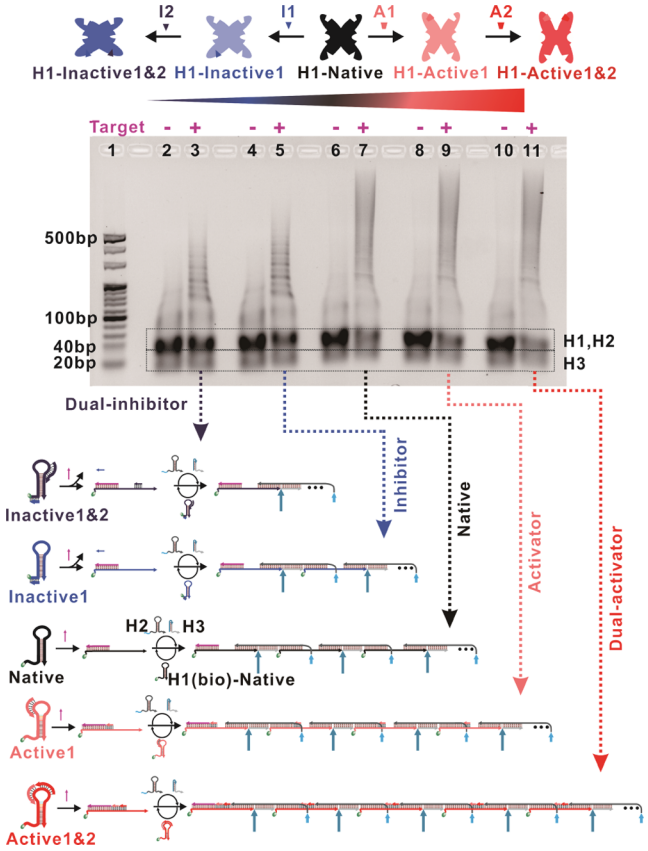

Figure 4. Analysis by AGE of the hybridization chain reaction regulated by single-effector allostery and dual-effector allostery. Lane 1, 20 bp DNA ladder markers; lanes 2 and 3, H1 + inhibitor1 + inhibitor2 + H2 + H3 + 0 or 0.1 μM target; lanes 4 and 5, H1 + inhibitor1 + H2 + H3 + 0 or 0.1 μM target; lanes 6 and 7, H1 + H2 + H3 + 0 or 0.1 μM target; lanes 8 and 9, H1 + activator1 + H2 + H3 + 0 or 0.1 μM target; and lanes 10 and 11, H1 + activator1 + activator2 + H2 + H3 + 0 or 0.1 μM target. [H1] = [H2] = [H3] = [inhibitor1/2] = [activator1/2] = 1 μM.

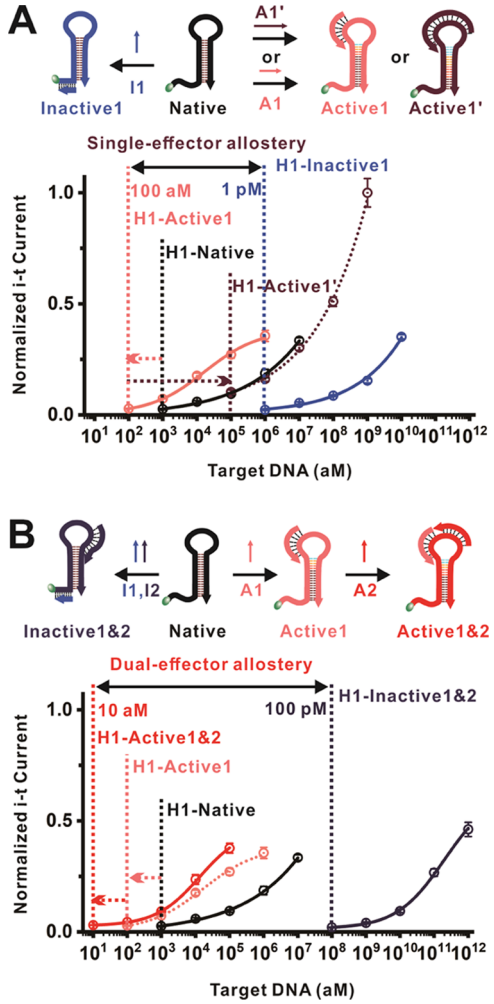

Figure 5. Rational design of allosterically inhibited and activated biosensors. (A) Dynamic detection range was tuned though single-effector allostery regulation. [Activator1] = [activator1′] = [inhibitor1] = 400 nM. (B) Dynamic detection range was tuned though dual-effector allostery regulation. [Activator1] = [activator2] = [inhibitor1] = [inhibitor2] = 200 nM.

nucleic acid detection with varied sensitivities (Figure 5A). As a result, the native target detection limit of the electrochemical sensor was 1 fM (Figure S9, (signal) ≥ (noise + 3 SD)). With 8 nt activator1, we can lower this detection limit to 100 aM. In contrast, 8 nt inhibitor1 produced a detection limit of 1 pM, such that our electrochemical sensor could achieve a range of nucleic acid detection limits from 100 aM to 1 pM. With a 16 nt activator1′, the detection limit increased to 100 fM due to the dramatically generated background. As expected, the detection limit range could be enlarged to 1000-fold greater by applying dual-effector allosteric cooperativity (Figure 5B, 10 aM to 100 pM). Using the dual-effector allostery modulating approach, we demonstrated that our electrochemical biosensor could analyze nucleic acid with a higher detection limit and a wider dynamic range spanning from as low as 10 aM to as high as 1 μM. Moreover, AGE analysis showed that the average lengths of the resulting multibranched HCR products were gradually reduced with the increase in the dual-inhibitor concentration (Figure S10). The detection limit of the electrochemical sensor also could be fine-tuned by varying the single-inhibitor or dual-inhibitor concentrations (Figure S11).

CONCLUSIONS

Here, we have proposed a new dual-effector allostery tool and demonstrated its advanced activation/inhibition performance. Using A dual-effector allostery-regulated multibranched hybridization chain reaction, we have developed an electrochemical biosensor for sensing target nucleic acid with a large-scale dynamic range. Compared to the single-effector allostery tool, the dual-effector allostery proposed here shows enhanced detection sensitivity and an extended dynamic range (10 aM to 1 μM). The introduction of the multivalent proximity ligation assay and the multivalent binding assay can further promote the sensitive detection of nucleic acid at ultralow concentrations. In addition, the dual-effector allostery strategy is the first update to the present toolbox of artificial allosteric regulation by mimicking newly found dual allosteric regulation in nature. It has the potential to enrich DNA complex designs with unprecedented property, a feature that can be of great potential in other fields.

https://doi.org/10.1021/acs.analchem.1c00055
Anal. Chem. 2021, 93, 8170−8177

■ ASSOCIATED CONTENT

Supporting Information

The Supporting Information is available free of charge at https://pubs.acs.org/doi/10.1021/acs.analchem.1c00055.

The table of sequences, the fluorescence assay mechanism, SNR of fluorescent analysis regulated by different concentrations of the effector, the effect of inhibitor2 alone, AGE analysis demonstration, electrochemical detection condition optimization, the electrocatalytic $i-t$ signal of the blank, and the nucleic acid detection regulated by different concentrations of inhibitors (PDF)

■ AUTHOR INFORMATION

Corresponding Authors

Guobao Zhou − *College of Biological, Chemical Sciences and Engineering, Jiaxing University, Jiaxing 314001, P. R. China;* orcid.org/0000-0002-6528-8290; Email: gbzhou@mail.zjxu.edu.cn

Lei Li − *College of Biological, Chemical Sciences and Engineering, Jiaxing University, Jiaxing 314001, P. R. China;* orcid.org/0000-0002-3357-337X; Email: lei.li@mail.zjxu.edu.cn

Huaping Peng − *Department of Pharmaceutical Analysis, Faculty of Pharmacy, Fujian Medical University, Fuzhou 350108, P. R. China;* orcid.org/0000-0003-3233-8877; Email: penghuaping@fjmu.edu.cn

Authors

Liangliang Liu − *Institute of Bast Fiber Crops, Chinese Academy of Agricultural Sciences, Changsha 410205, P. R. China*

Mengmeng Yuan − *College of Biological, Chemical Sciences and Engineering, Jiaxing University, Jiaxing 314001, P. R. China*

Yuxia Jin − *College of Biological, Chemical Sciences and Engineering, Jiaxing University, Jiaxing 314001, P. R. China*

Tuqiang Li − *College of Biological, Chemical Sciences and Engineering, Jiaxing University, Jiaxing 314001, P. R. China*

Wei Chen − *Department of Pharmaceutical Analysis, Faculty of Pharmacy, Fujian Medical University, Fuzhou 350108, P. R. China*

Complete contact information is available at: https://pubs.acs.org/10.1021/acs.analchem.1c00055

Author Contributions

‖L. Liu and M.Y. contributed equally to this work.

Notes

The authors declare no competing financial interest.

■ ACKNOWLEDGMENTS

This work was supported by the National Natural Science Foundation of China (Nos. 21677060 and 21874020), the Zhejiang Provincial Natural Science Foundation of China (No. LQ19B050002), the grants from the Public Welfare Technology Research Program of Zhejiang Province (No. LGF18H040008), the Program for Science and Technology of Jiaxing (No. 2019AY11009), and the start-up fund of the Jiaxing University (70518013).

■ REFERENCES

(1) Rolfo, C.; Russo, A. *Nat. Rev. Clin. Oncol.* **2020**, *17*, 523−524.

(2) Zhao, Y.; Liu, H.; Chen, F.; Bai, M.; Zhao, J.; Zhao, Y. *Biosens. Bioelectron.* **2016**, *86*, 892−898.

(3) Wagner, P. D.; Verma, M.; Srivastava, S. *Ann. N. Y. Acad. Sci.* **2004**, *1022*, 9−16.

(4) Heidary, M.; Auer, M.; Ulz, P.; Heitzer, E.; Petru, E.; Gasch, C.; Riethdorf, S.; Mauermann, O.; Lafer, I.; Pristauz, G.; Lax, S.; Pantel, K.; Geigl, J. B.; Speicher, M. R. *Breast Cancer Res.* **2014**, *16*, No. 421.

(5) De Rubis, G.; Rajeev Krishnan, S.; Bebawy, M. *Trends Pharmacol. Sci.* **2019**, *40*, 172−186.

(6) Jin, D.; Peng, X. X.; Qin, Y.; Wu, P.; Lu, H.; Wang, L.; Huang, J.; Li, Y.; Zhang, Y.; Zhang, G. J.; Yang, F. *Anal. Chem.* **2020**, *92*, 9877−9886.

(7) Yang, F.; Zuo, X. L.; Li, Z. H.; Deng, W. P.; Shi, J. Y.; Zhang, G. J.; Huang, Q.; Song, S. P.; Fan, C. H. *Adv. Mater.* **2014**, *26*, 4671−4676.

(8) Jacobs, J. M.; Adkins, J. N.; Qian, W. J.; Liu, T.; Shen, Y.; Camp, D. G.; Smith, R. D. *J. Proteome Res.* **2005**, *4*, 1073−1085.

(9) Mitchell, P. S.; Parkin, R. K.; Kroh, E. M.; Fritz, B. R.; Wyman, S. K.; Pogosova-Agadjanyan, E. L.; Peterson, A.; Noteboom, J.; O'Briant, K. C.; Allen, A.; Lin, D. W.; Urban, N.; Drescher, C. W.; Knudsen, B. S.; Stirewalt, D. L.; Gentleman, R.; Vessella, R. L.; Nelson, P. S.; Martin, D. B.; Tewari, M. *Proc. Natl. Acad. Sci. U.S.A.* **2008**, *105*, 10513−10518.

(10) Wan, J. C. M.; Heider, K.; Gale, D.; Murphy, S.; Fisher, E.; Mouliere, F.; Ruiz-Valdepenas, A.; Santonja, A.; Morris, J.; Chandrananda, D.; Marshall, A.; Gill, A. B.; Chan, P. Y.; Barker, E.; Young, G.; Cooper, W. N.; Hudecova, I.; Marass, F.; Mair, R.; Brindle, K. M.; Stewart, G. D.; Abraham, J. E.; Caldas, C.; Rassl, D. M.; Rintoul, R. C.; Alifrangis, C.; Middleton, M. R.; Gallagher, F. A.; Parkinson, C.; Durrani, A.; McDermott, U.; Smith, C. G.; Massie, C.; Corrie, P. G.; Rosenfeld, N. *Sci. Transl. Med.* **2020**, *12*, No. eaaz8084.

(11) Kang, B.; Park, S. V.; Soh, H. T.; Oh, S. S. *ACS Sens.* **2019**, *4*, 2802−2808.

(12) Drabovich, A. P.; Okhonin, V.; Berezovski, M.; Krylov, S. N. *J. Am. Chem. Soc.* **2007**, *129*, 7260−7261.

(13) Kimoto, M.; Shermane Lim, Y. W.; Hirao, I. *Nucleic Acids Res.* **2019**, *47*, 8362−8374.

(14) Vallée-Bélisle, A.; Ricci, F.; Plaxco, K. W. *J. Am. Chem. Soc.* **2012**, *134*, 2876−2879.

(15) Ricci, F.; Vallée-Bélisle, A.; Porchetta, A.; Plaxco, K. W. *J. Am. Chem. Soc.* **2012**, *134*, 15177−15180.

(16) Porchetta, A.; Vallée-Bélisle, A.; Plaxco, K. W.; Ricci, F. *J. Am. Chem. Soc.* **2012**, *134*, 20601−20604.

(17) Zidong, W.; Heon, L. J.; Yi, L. *Adv. Mater.* **2008**, *20*, 3263−3267.

(18) Liu, J.; Lu, Y. *J. Am. Chem. Soc.* **2003**, *125*, 6642−6643.

(19) Marvin, J. S.; Corcoran, E. E.; Hattangadi, N. A.; Zhang, J. V.; Gere, S. A.; Hellinga, H. W. *Proc. Natl. Acad. Sci. U.S.A.* **1997**, *94*, 4366−4371.

(20) Lu, X.; Zhou, G.; Zeng, Y.; Yin, Z.; Zhang, Z.; Guo, L.; Zhai, Y.; Yang, Y.; Wang, H.; Li, L. *Chem. Sci.* **2019**, *10*, 5025−5030.

(21) Xianyu, Y.; Wu, J.; Chen, Y.; Zheng, W.; Xie, M.; Jiang, X. *Angew. Chem., Int. Ed.* **2018**, *57*, 7503−7507.

(22) Pu, F.; Huang, Z.; Ren, J.; Qu, X. *Anal. Chem.* **2010**, *82*, 8211−8216.

(23) Li, C. M.; Zhen, S. J.; Wang, J.; Li, Y. F.; Huang, C. Z. *Biosens. Bioelectron.* **2013**, *43*, 366−371.

(24) Noor, M. O.; Krull, U. J. *Anal. Chem.* **2013**, *85*, 7502−7511.

(25) Smith, L.; Kohli, M.; Smith, A. M. *J. Am. Chem. Soc.* **2018**, *140*, 13904−13912.

(26) Jang, H. R.; Wark, A. W.; Baek, S. H.; Chung, B. H.; Lee, H. J. *Anal. Chem.* **2014**, *86*, 814−819.

(27) Renard, M.; Bedouelle, H. *Biochemistry* **2004**, *43*, 15453−15462.

(28) Lu, X.; Wang, L.; Chen, Q.; Wang, Y.; Cao, Z.; Zhou, G.; Li, L. *Chem. Commun.* **2020**, *56*, 4184−4187.

(29) Nguyen, B. L.; Jeong, J. E.; Jung, I. H.; Kim, B.; Le, V. S.; Kim, I.; Kyhm, K.; Woo, H. Y. *Adv. Funct. Mater.* **2014**, *24*, 1748−1757.

(30) Xiang, Y.; Tong, A.; Lu, Y. *J. Am. Chem. Soc.* **2009**, *131*, 15352−15357.
(31) Zheng, X.; Yang, J.; Zhou, C.; Zhang, C.; Zhang, Q.; Wei, X. P. *Nucleic Acids Res.* **2019**, *47*, 1097−1109.
(32) Urlinger, S.; Baron, U.; Thellmann, M.; Hasan, M. T.; Bujard, H.; Hillen, W. *Proc. Natl. Acad. Sci. U.S.A.* **2000**, *97*, 7963−7968.
(33) Porchetta, A.; Vallée-Bélisle, A.; Plaxco, K. W.; Ricci, F. *J. Am. Chem. Soc.* **2013**, *135*, 13238−13241.
(34) Song, P.; Li, M.; Shen, J. W.; Pei, H.; Chao, J.; Su, S.; Aldalbahi, A.; Wang, L. H.; Shi, J. Y.; Song, S. P.; Wang, L. H.; Fan, C. H.; Zuo, X. L. *Anal. Chem.* **2016**, *88*, 8043−8049.
(35) Brown, J. A.; Thorpe, I. F. *Biochemistry* **2015**, *54*, 4131−4141.
(36) Asención Diez, M. D.; Aleanzi, M. C.; Iglesias, A. A.; Ballicora, M. A. *PLoS One* **2014**, *9*, No. e103888.
(37) Fodor, M.; Price, E.; Wang, P.; Lu, H.; Argintaru, A.; Chen, Z.; Glick, M.; Hao, H.-X.; Kato, M.; Koenig, R.; LaRochelle, J. R.; Liu, G.; McNeill, E.; Majumdar, D.; Nishiguchi, G. A.; Perez, L. B.; Paris, G.; Quinn, C. M.; Ramsey, T.; Sendzik, M.; Shultz, M. D.; Williams, S. L.; Stams, T.; Blacklow, S. C.; Acker, M. G.; LaMarche, M. J. *ACS Chem. Biol.* **2018**, *13*, 647−656.
(38) Zhang, X. L.; Yang, Z. H.; Chang, Y. Y.; Qing, M.; Yuan, R.; Chai, Y. Q. *Anal. Chem.* **2018**, *90*, 9538−9544.

https://doi.org/10.1021/acs.analchem.1c00055
Anal. Chem. 2021, 93, 8170−8177